Urban Impervious Surface Estimation from Remote Sensing and Social Data

Yan Yu, Jun Li, Changyu Zhu, and Antonio Plaza

Abstract

We propose an inspiring approach for accurate impervious surface estimation based on the integration of remote sensing and social data. The proposed approach exploits the strengths of two kind of heterogeneous features, i.e., physical features and social features, where the former ones are derived by a morphological attribute profiles-guided spectral mixture analysis model using remote sensing imagery, and the latter ones are obtained from the normalized kernel density of point of interest and vector road datasets. These two features are then integrated using a multivariable linear regression model to estimate impervious surfaces. The proposed method has been tested in the main urban area of Guangzhou, China, in pixel level and parcel level, respectively. The obtained results, with the overall RMSE of 10.98% and 10.90% for pixel level and parcel level, respectively, demonstrate the good performance of integrating remote sensing imagery and social data for mapping of urban impervious surface.

Introduction

Impervious surfaces (IS), defined as the surfaces that water cannot infiltrate, are usually made up of anthropogenic materials, e.g., rooftops, parking lots, streets, and outdoor facilities (Slonecker *et al.*, 2001). These increasing IS have been identified as a significant indicator of ecological condition and urbanization (Brabec *et al.*, 2002; Hasse and Lathrop, 2003), as they have direct impacts on water quality of neighboring water bodies, hydrologic cycles, natural temperature cycles, and land surface temperatures (Schueler, 1994; Adams *et al.*, 1993; Geiger *et al.*, 2009; Yuan and Bauer, 2007). The demand for current and accurate IS maps has greatly increased. To date, different approaches have been applied to characterize and quantify IS using ground-measured data and remote sensing data (Weng, 2012).

Remote sensing data have been used for the estimation of IS since the 1970s. Many techniques have been proposed to exploit the spatial, spectral, texture and context information of remote sensing data (Weng, 2012). For instance, Møller-Jensen (1990) applied a linear segmentation model which incorporates texture and context information of Landsat-TM imagery to cover urban areas. Deng *et al.* (2012) used a linear spectral un-mixing model to extract IS information from Landsat imagery. Research on imperviousness estimation from multi-sensor and multi-source data has also attracted interest. Yang *et al.* (2003) quantified urban IS by using Landsat-7 ETM+ and high-resolution imagery. Liu *et al.* (2013) integrated night-time light luminosity, land surface temperature and multi-spectral reflectance data to enhance IS while suppressing other unwanted land covers. Huang *et al.* (2017) studied the subtle urban changes using multi-view satellite imagery. Although remote sensing data brings desirable properties (large coverage, information of spectral reflectance, etc.), impervious surface estimation is still a difficult task due to the complexity of urban/suburban land cover, as well as the limitations of spectral and spatial resolution of remote sensing imagery (Lu and Weng, 2006). In this sense, medium-resolution satellite imagery can help to map urbanization areas at a large spatial scale, but it may lead to the underestimation of IS because of the heterogeneity of urban landscapes (e.g., soil, grass and water body). High-resolution remote sensing imagery (Ikonos, GF-2, aerial photography, etc.), provides an alternative. Numerous pixel-based methods and object-based methods have been explored to map the IS with high-resolution imagery. Sawaya *et al.* (2003) utilized several pixel-based methods to map the imperviousness of Eagan City. Lu and Weng (2006) estimated urban impervious surface using decision tree classifier and linear spectral mixture analysis model. Li *et al.* (2011) explored the object-based method to map urban impervious surface using very high resolution imagery. Zhang and Huang (2018) monitored the change of impervious surface using the multi-feature objected-based approach. In general, the accuracy of impervious fractions generated by traditional estimation methods, such as those presented in Bauer *et al.*, 2004; Lu *et al.*, 2011; Wu and Murray, 2003, is mostly dependent on the quality of multi/hyper-spectral imagery. These signature-based methods however have limitations in low-albedo imperviousness like old town areas, shadow, and urban greening areas.

The fast development of social technologies with global navigation satellite system results in a wide availability of social data, such as taxi GPS data, smart card data, social media data, and volunteered web maps. These heterogeneous datasets, with the attributes of geographic and human activity, provide unprecedented possibilities for the improvement of urban study (Hu *et al.*, 2016; Liu *et al.*, 2015; Lu and Liu, 2012). Point of interest (POI) data, composed of geographic location and their particular place-based information are widely available on the Web like *Google Place*[1], *Facebook Place*[2], *Gaode Place*[3] (in China), which use their own taxonomy of categories or tags (Rodrigues *et al.*, 2012). Different from the check-in data gathered from social media platforms, POI data are usually associated with their certain and detailed information as names, addresses, coordinates (latitudes and longitudes), categories, etc., which can reflect the land use type of a certain place. They therefore provide a new direction for

1. http://www.google.com/places/
2. https://www.facebook.com/about/location/
3. http://www.openstreetmap.org

Yan Yu, Jun Li, and Changyu Zhu are with the Guangdong Provincial Key Laboratory of Urbanization and Geo-simulation, School of Geography and Planning, Sun Yat-sen University, Guangzhou, 510275, China (corresponding author: Jun Li; lijun48@mail.sysu.edu.cn)

Antonio Plaza is with the Hyperspectral Computing Laboratory, Department of Technology of Computers and Communications, Escuela Politécnica de Cáceres, University of Extremadura, Cáceres, Spain.

Photogrammetric Engineering & Remote Sensing
Vol. 84, No. 12, December 2018, pp. 771–780.
0099-1112/18/771–780

doi: 10.14358/PERS.84.12.771

urban study, particularly for urbanization monitoring, with the aim to identify and classify the land use type (Rodrigues *et al.*, 2012). Jiang *et al.* (2015) utilized volunteered POI data to estimate the land use at census block level. Hu *et al.* (2016) integrated Landsat imagery and open social data to map the urban land use of Beijing, China. *OpenStreetMap*[4] (*OSM*) is a collaborative mapping project where maps are collected and upload by volunteers. As the pioneer project of Volunteered Geographic Information, *OSM* has provided a large volume of fully open-source and editable geographical data including roads, waterways, railways, and buildings. Currently, *OSM* data have become a popular data source and have been widely used in urban issue, such as the research in Arsanjani *et al.*, 2013 and Johnson and Iizuka, 2016. These studies, although limited, suggest a strong potential to integrate the remote sensed features with social knowledge.

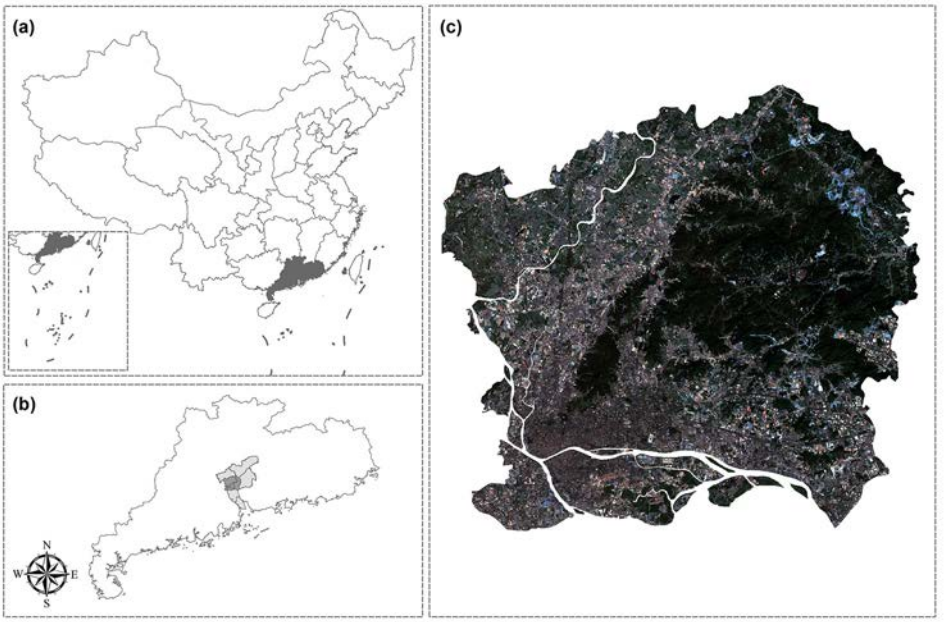

Figure. 1. (a) Guangdong province, located in the south of China, (b) Guangzhou City, the capital city of Guangdong province, is the main economic hub of the Pearl River Delta, and (c) Remote sensing imagery of our study area, acquired by *Landsat-8* satellite.

Remote sensing is an effective technology to map the ground with large coverage, but the latest and high-resolution remote sensing imagery is not easy to access. On the other hand, social data, with the attributes of geographic and human activity characteristics, constitute an interesting source of information. In this paper, a new technique for the estimation of IS, taking advantage of both remote sensing data and social data, is developed. Morphological attribute profiles (MAPs) (Dalla Mura *et al.*, 2010) is an advanced tool for spatial features extraction from remote sensing imagery, while spectral mixture analysis (SMA)-based methods are effective to evaluate the characterization of IS. In this work, we adopt MAPs of four structural attributes (area, length of bounding box, standard deviation, and moment of inertia) into a SMA model to generate physical features from multi-spectral remote sensing imagery. On the other hand, we apply a normalized kernel density estimation (KDE) model (Silverman, 1986) to estimate the social features of IS using POI datasets. To further enhance the urban structure information, road network datasets are considered in our experiments. Finally, we use a multivariable linear regression model (LRM) for feature integration in two different level, i.e. pixel level and parcel level.

The reminder of this paper is structured as follows. The next Section 2 introduces the study area and the datasets adopted in our experimentsfollowed by our methodological approach in detail. The experimental results and discussions are then demonstrated. Finally, we conclude the paper with some remarks and hints at plausible future research

Study Area and Datasets

Study Area

Guangzhou, located in the south of China (112°57′ E~114°3′ E and 22°26′ N~23°56′ N), is one of the most populated cities (with a population of 14.04 million). As the capital city and the major port of Guangdong province, Guangzhou experienced rapid development during the past 30 years. In this research, we selected the central parts of Guangzhou City as our study area, which cover several typical urban land use categories including impervious surfaces such as commercial land, residential land, road, and parking lot, as well as pervious surfaces such as park, forest, grassland, and bare soil (Figure 1).

Data Collection and Preprocessing

Remote Sensing Data

We adopted *Landsat-8* Operational Land Imager (OLI) imagery (path 122/row 44) of Guangzhou acquired on 23 October, 2017, as our remote sensing data source. This multi-spectral imagery, provided by U.S. Geological Survey[5], has eight reflective bands of 30 m spatial resolution and one panchromatic band of 15 m spatial resolution, with a low cloud coverage proportion of 5%. This imagery was corrected with ground control points and projected into UTM WGS84 coordinate system. After that, this dataset was converted to normalized exo-atmospheric reflectance measures with the radiance to reflectance conversion formula (Markham and Barker, 1987). Also, all water bodies were masked out. Moreover, high-resolution images on *Gaode Map* were used to collect the reference data for training and accuracy validation, under the assumption that there were no apparent changes happened among *Landsat* imagery and online map due to the close acquisition time.

Social Data

We gathered more than one million POIs of Guangzhou from *Gaode Map* by using an application programming interface[6]. Each POI contains certain locational and functional information, i.e. ID, category, and coordinate (latitude and longitude) of a place. Different from the volunteered geographic information collected from social media platforms like *Facebook*, *Twitter* or *Sina Weibo* (Chinese *Twitter*), the POI data used in this work have already been collected, sorted, and verified by the surveying and mapping team of *Gaode Map* by 23 June, 2016. It should be noticed that the acquisition time of remote

4. http://lbs.amap.com/api/webservice/guide/api/search/

5. http://earthexplorer.usgs.gov/

6. http://lbs.amap.com/api/

sensing data and social data should be as close as possible, because of the continuous construction of a city. The initial 864 types of POIs were gathered into 2 categories (see Table 1) including impervious point dataset (683,161 POIs) and pervious point dataset (1,337 POIs), as shown in Figure 2a. POIs that did not belong to these two categories were removed. It should be noted that, with a total number of 684,496 impervious and pervious POIs, the distribution of POIs, although biased, i.e., there are less POIs in sub-urban areas than that in urban areas, is good enough for the exploration of the complementary of remote sensing and social data.

Also we collected the road network of study area from *OSM* (Figure 2b)). This vector dataset has been recognized and classified by street function/level (e.g., motorway, primary, secondary, trunk, tertiary, residential, service, footway ,and relief road).

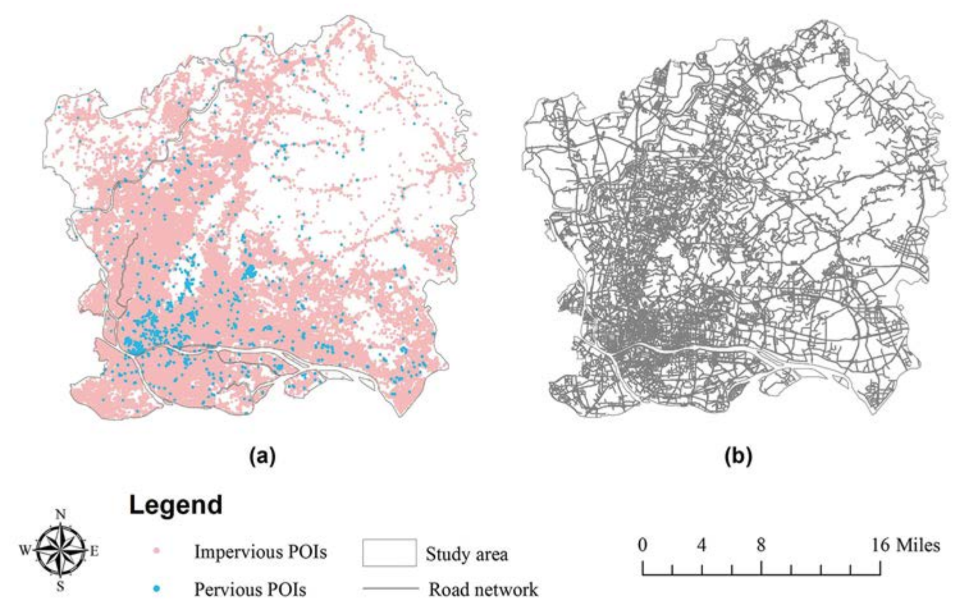

Figure 2. (a) POIs of imperviousness and perviousness, and (b) Road network acquired from OSM.

Table 1. POI classification system.

Class I	Class II	Descriptions
Impervious POIs	Industrial	Warehousing, manufacturing, recycling
	Commercial	Automotive service, restaurant place, department store, shopping center, hotel
	Institutional	Government service, transportation, sports complex, hospital, educational place, cultural venues and facilities
	Residential	Community, service apartment
Pervious POIs	Water body	Lake, river
	Green space	Park, scenic spot, tourist area

Methodology

Urban parcel, which can be bounded by road network, is defined as the basic spatial unit carrying the social functions in urban management and urban planning (Hu *et al.*, 2016). Recently, parcel based urban study models are widely applied to better describe the urban function and capture the comprehensive and strategic urban planning (Liu and Long, 2016). Urban parcel has been proved to be an effective data source in urban function description (Yuan *et al.*, 2012), which has been a tremendous benefit to support urban management decision-making. So in this work, we conducted two IS estimation experiments, i.e., pixel-based IS estimation and parcel-based IS estimation to better present the contributions brought by POIs and road network while seeing the differences between the pixel-based and parcel-based method.

The framework of our proposed approach is illustrated in Figure 3. First, we adopt MAPs and build four structural attributes (area, length of bounding box, standard deviation, and moment of inertia) that are then fed to a SMA model to estimate the physical features of urban IS from Landsat-8 imagery. Then, in the processing of social data, we extract two kinds of social features based on pixel-level and parcel-level. These two set of features (pixel-based and parcel-based features) are then fused into a multivariable LRM, respectively, to provide an estimation of IS. In the following, we detail each step of the adopted method.

Physical Features Extraction

In this study, the physical features are derived by using a morphological attribute profiles-guided spectral mixture analysis model following the previous successful instructions (Zhu *et al.*, 2018). It should be note that, physical information is reserved in some aspects by feeding the original bands of multispectral imagery into MAPs. Meanwhile, previous studies (Zhu *et al.*, 2018) as well as our experiment results have shown its promising performance with a acceptable accuracy in physical feature extraction. Nevertheless, how to interpret its physical information is still a remaining challenge. Future efforts can be undertaken for further improvement.

According to Zhu *et al.* (2018), first we extract the spatial features from remote sensing imagery using MAPs with four different structural attributes, including area, length of bounding box, standard deviation, and moment of inertia. MAPs are derived by generating the attribute profile (AP) on each band of multispectral imagery. For pixel x_i, MAP can be defined as:

$$\text{MAP}(I) = \{AP(I_1), AP(I_2), \ldots, AP(I_P)\} \quad (1)$$

where $AP(I_P)$ is the attribute profile of feature p. These spatial features derived above are then fed to an SMA model to estimate the multiple spectral signatures and their corresponding abundance. As Wu and Murray (2003) suggested that the impervious surfaces are likely to be the combination of high-albedo and low-albedo fraction images, we consider the high and low albedo endmembers to linearly represent the initial impervious fractions, which is given by:

$$F_b = \omega_{low}, F_{low,b} + \omega_{high}, F_{high,b} + e_b \quad (2)$$

where F_b is the initial impervious fractions of band b, $F_{low,b}$ and $F_{high,b}$ are the low-albedo and high-albedo spectra of band b, ω_{low} and ω_{high} are the weight of low-albedo and high-albedo, respectively, and e_b is the un-modeled residual. Equation 2 should follow the assumption that $\omega_{low} + \omega_{high} = 1$ while ω_{low}, $\omega_{high} \geq 0$. In this work, we consider the obtained initial impervious fractions as the physical features of remote sensing imagery. This leads to the following definition of physical features:

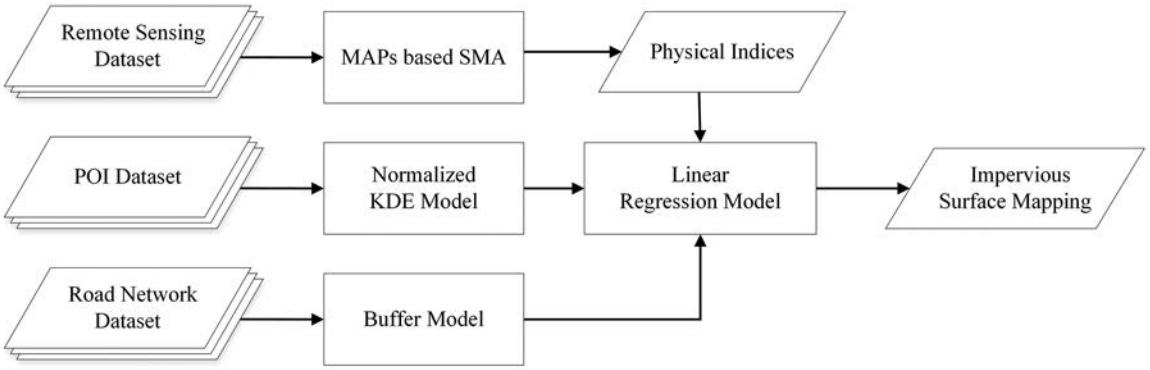

Figure 3. Graphical illustration of the proposed approach.

$$f_1 = \{F_1, F_2, \ldots, F_b\}. \quad (3)$$

It might also be note that parameters of Equations 1 and 2 are selected following Zhu *et al.* (2018). The physical features of Landsat-8 imagery are shown in Figure 4a.

Social Data Processing

POI Dataset

Kernel density estimation (KDE) model (Silverman, 1986) is an effective technique to converse independent points into continuous density map with a proper radius of influence (Meng *et al.*, 2017). This technique is widely used in identifying city functions (Yuan *et al.*, 2012), flood assessment (Schnebele, 2013), land over change detection (Meng *et al.*, 2017), etc. In this work, we use KDE model to estimate the distributions of impervious and pervious POIs, respectively, as follows:

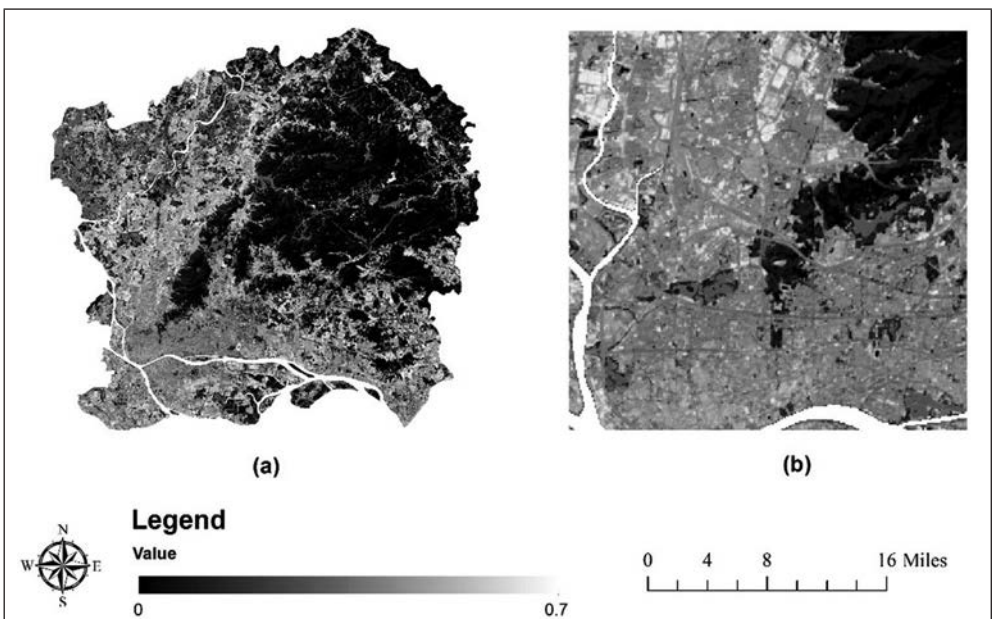

Figure 4. (a) Physical features of *Landsat-8* imagery, and (b) is the zoomed-in view of old town area (Yuexiu district). This area holds the low impervious fractions for the existence of countless tree crowns and parks.

$$M(x) = \frac{1}{pnh}\sum_{i=1}^{n} K\left(\frac{x - x_i}{h}\right) \quad (4)$$

where $\{x_1, \ldots, x_n\}$ are the set of n independent POIs, k is the quartic (biweight) kernel function given by:

$$K(u) = \frac{3}{\pi}\left(1 - u^2\right)^2 \quad (5)$$

while $|u| \leq 1$. h is the search radius, which is generally set according to the spatial resolution of remote sensing imagery and the distribution of the POIs. In this work, we implement the KDE model to generate the intensity of impervious POIs and pervious POIs with the search radius of 200m and 400m, respectively. Due to the huge gap of data quantity among these two POI datasets, we normalize two density maps by (Hu *et al.*, 2016):

$$f_{2,3} = \left(M - M_{\min}\right) / \left(M_{\max} - M_{\min}\right), \quad (6)$$

where f_2 and f_3 are the normalized kernel density maps of impervious and pervious POIs, respectively. Two smooth maps indicate the density of two POI datasets, and pixels/regions with higher density values mean that there are more POIs, see Figure 6.

Processing of the Road Network Dataset

In this study, to simulate road covers, we buffer the road network with different road widths, e.g., 25 m, 20 m, 20 m, 15 m, and 10 m for motorway, primary, secondary, tertiary and residential, respectively, referring to China Ministry of Housing and Urban-Rural Development[7], see Figure 5a. Then, 10,978 vector urban parcels are generated after removing road spaces (Figure 5b).

Feature Integration

A multivariable linear regression model is implemented to fuse the obtained physical and social features, as follows:

$$IS_i = \omega_1 f_{1i} + \omega_2 f_{2i} + \ldots + \omega_n f_{ni}, \quad (7)$$

where f_n presents the abundance map of feature n. ω_n is the parameter controlling the weight of feature n. In this work, we select 100 training samples (90 m × 90 m) to learn the weight of each feature based on least square method. Then,

7. http://www.mohurd.gov.cn/

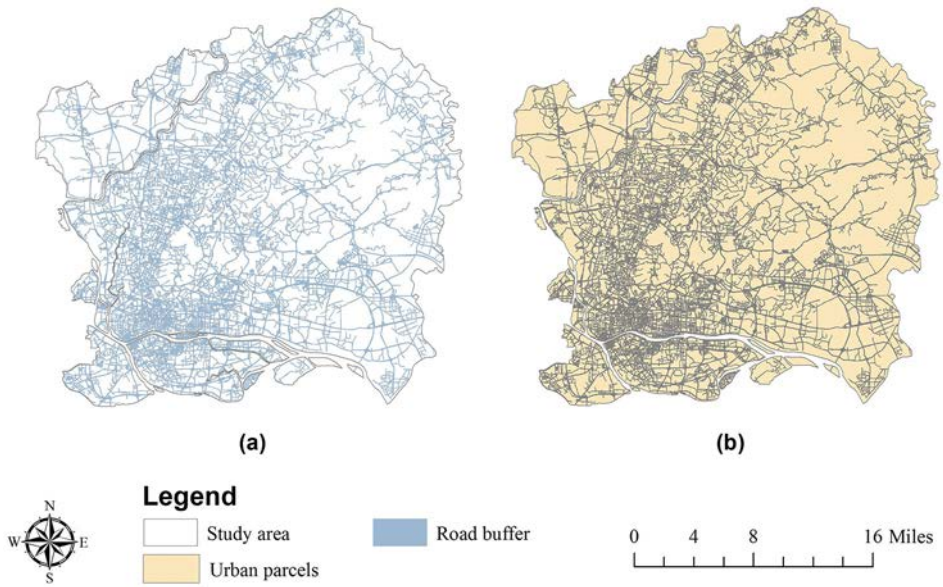

Figure 5. (a) Road map derived by road network, (b) Urban parcels of study area.

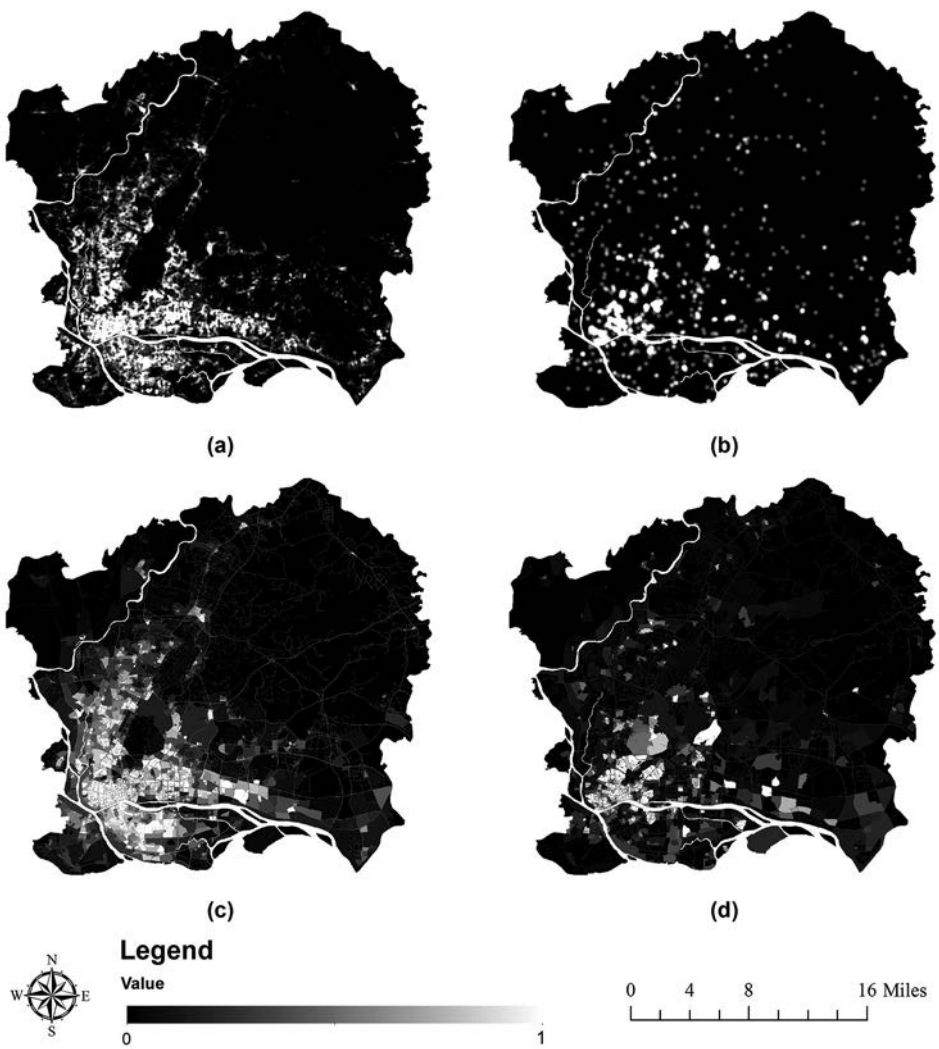

Figure 6. Pixel-based normalized kernel density maps of (a) impervious POIs, and (b) pervious POIs. Parcel-based normalized kernel density maps of (c) impervious POIs and (d) pervious POIs.

these learned weights are utilized to reconstruct impervious fraction map.

Accuracy Assessment

The general accuracy indicator used in this work is the R-square, given by:

$$R^2 = \frac{SSR}{SST} \tag{8}$$

in which *SSR* is the regression sum of squares and *SST* is the total sum of squares. The higher R-square suggests the less similarity difference among impervious fractions derived by the proposed approach and reference data. Furthermore, another three error measurements (1) root mean square error (RMSE), (2) mean absolute error (MAE), and (3) systematic error (SE) are used to evaluate the accuracy of our technique in detail, which are respectively given by:

$$RMSE = \sqrt{\frac{1}{n}\sum_{i=1}^{n}\left(\Gamma(x_i) - \hat{\Gamma}(x_i)\right)^2}\ , \tag{9}$$

$$MAE = \frac{1}{n}\sum_{i=1}^{n}\left|\Gamma(x_i) - \Gamma(x_i)\right|\ , \tag{10}$$

$$SE = \frac{1}{n}\sum_{i=1}^{n}\left(\Gamma(x_i) - \hat{\Gamma}(x_i)\right)\ , \tag{11}$$

where Γ represents the final output of our proposed method, $\hat{\Gamma}$ is the reference impervious fractions (in this study, we interpreted the reference data from *Gaode Map Online*). RMSE and MAE predict the estimation errors, and SE indicates the overall tendency of the estimation bias.

Experimental Results

Two different experiments were conducted. The next Section presents the pixel-based IS estimation experiment, followed by the parcel-based IS estimation experiment. 150 patches (90 m × 90m) were randomly collected for accuracy assessment. These samples are with a good coverage over the study area among all the land use types including roads, residential areas, business blocks, vegetation, and shadows.

Pixel-based Impervious Surface Estimation

Figure 7a illustrates the IS result estimated from physical features and POI features. Meanwhile, we considered the road distribution map (see Figure 5a) as an additional source of social data, and then fed all physical and social features into IS estimation model (The result is shown in Figure 7b). The fractions of (7a) and (7b) both vary from 0 to 1, and the learned weights of features are illustrated in Table 2. Figure 7c and 7d give the zoomed-in views of (7a) and (7b), respectively. Three fitting curves are drawn in Figure 7e reference data versus physical features (R-square = 0.6932), (7f) reference data versus impervious fractions integrating physical features and POI features (R-square = 0.8345), and (7g) reference data versus impervious fractions integrating physical features and all social features (R-square =0.8452), suggesting a strong correlation between the impervious fractions we obtained and the reference data. Three R-square values go from 0.6932 to 0.8345 and then up to 0.8345, which indicates the great contributions brought by POIs and road network. Because of the low coverage rate of road network and the randomness

Table 2. Feature weights learned by multivariable linear regression model.

		Experiment I	Experiment II
Pixel-based (section 4.1)	Physical Features	0.91	0.76
	Impervious POIs Features	0.59	0.49
	Pervious POIs Features	-0.11	-0.13
	Road Features		0.18
Parcel-based (section 4.2)	Physical Features	0.87	0.84
	Impervious POIs Features	0.79	0.76
	Pervious POIs Features	-0.09	-0.10
	Road Features		0.04

Table 3. Accuracy comparison between the physical features we extracted in 3.1 and our proposed method using RMSE, MAE and SE of two experiments.

Methods	Area	RMSE(%)	MAE(%)	SE(%)
Physical Features	Less Developed Area	12.09	6.70	-5.32
	Developed Area	18.08	14.23	13.68
	Overall	14.66	9.56	1.90
Pixel-based	Less Developed Area	10.65	6.65	-5.68
	Developed Area	11.49	9.03	6.41
	Overall	10.98	7.55	-1.09
Parcel-based	Less Developed Area	10.32	5.95	-4.78
	Developed Area	11.79	9.28	4.94
	Overall	10.90	7.21	-1.09

of samples, it is not easy to substantiate the contributions of road network by using the R-square value. However, by considering road distribution, we can capture each block clearly in the resulting map (Figure 7d).

Parcel-based Impervious Surface Estimation

In this paper, we consider the mean value of pixels in each parcel as the parcel-based physical features. Because of the complicated internal structure of each parcel, the accuracy of the parcel-based method is not as good as pixel-based method. Figure 8a shows the obtained impervious map integrating physical features and POI features, while Figure 8b takes the advantage of physical features, POI features and road distribution. The learned weights are shown in Table 2. Also, the enlarged views of these two maps with values varying from 0 to 1 are illustrated in Figure 8c and 8d. The following figures: (8e), (8f), and (8g) give the fitting curves of reference data versus physical features, reference data versus IS result using physical and POI features, and reference data versus impervious fractions integrating physical and all social features. Three R-square values are 0.6932, 0.7512, and 0.7529, respectively. The experimental results suggest that parcel-based methods contribute significantly to IS estimation. Furthermore, parcel-based methods are also promising for higher level decision making in urban planning and urban analysis.

Accuracy Assessment

To further evaluate the accuracy of our work, referring to Bauer *et al.* (2004), two types of land covers including developed areas and less developed areas are conducted for verification purposes. Based on the definition of impervious surface in (Arnold, Jr. and Gibbons, 1996) and the exact conditions of study area, pixels with values equal or larger than 0.4 are sorted into developed area, and the rest are allocated to less developed area. Meanwhile, in order to explore the benefits of social knowledge, we use the physical features previously extracted for comparison. Three considered error measurements (including RMSE, MAE, and SE) are listed in Table 3, revealing the persuasiveness and advancement of our method.

Generally, the accuracy of our work is persuasive. The overall RMSE is 10.98% and overall MAE is 7.55% in pixel-based experiment, while in parcel-based experiment, the overall RMSE is 10.90% and overall MAE is 7.21%. Compared with physical features (initial impervious fractions), our proposed method could well avoid the influence of tree crowns/shadows with a promising accuracy.

Discussion

In this study, we explored the potential of integrating remote sensing data and social knowledge in urban impervious surface estimation. Remote sensing is an efficient approach to map the biophysical characteristics of the Earth's surface. However, its performance strongly depends on the observation conditions. This is a critical issue in urbanization monitoring, for instance: (1) rooftops covered by vegetation canopies may be characterized as pervious in remote sensing imagery, and (2) impervious fractions of small parks hiding in the residential areas are easily influenced by the reflected lights of buildings. These could largely result in improper impervious fractions. While combined with social knowledge, these effects could be well avoided. Figure 9 gives an example of Yuexiu District, which is the old city town of Guangzhou. This area is mostly covered by big tree crowns, which leads to the low-albedo (varying from 0.3 to 0.5) in impervious fractions generated from remote sensing imagery (Figure 9b).

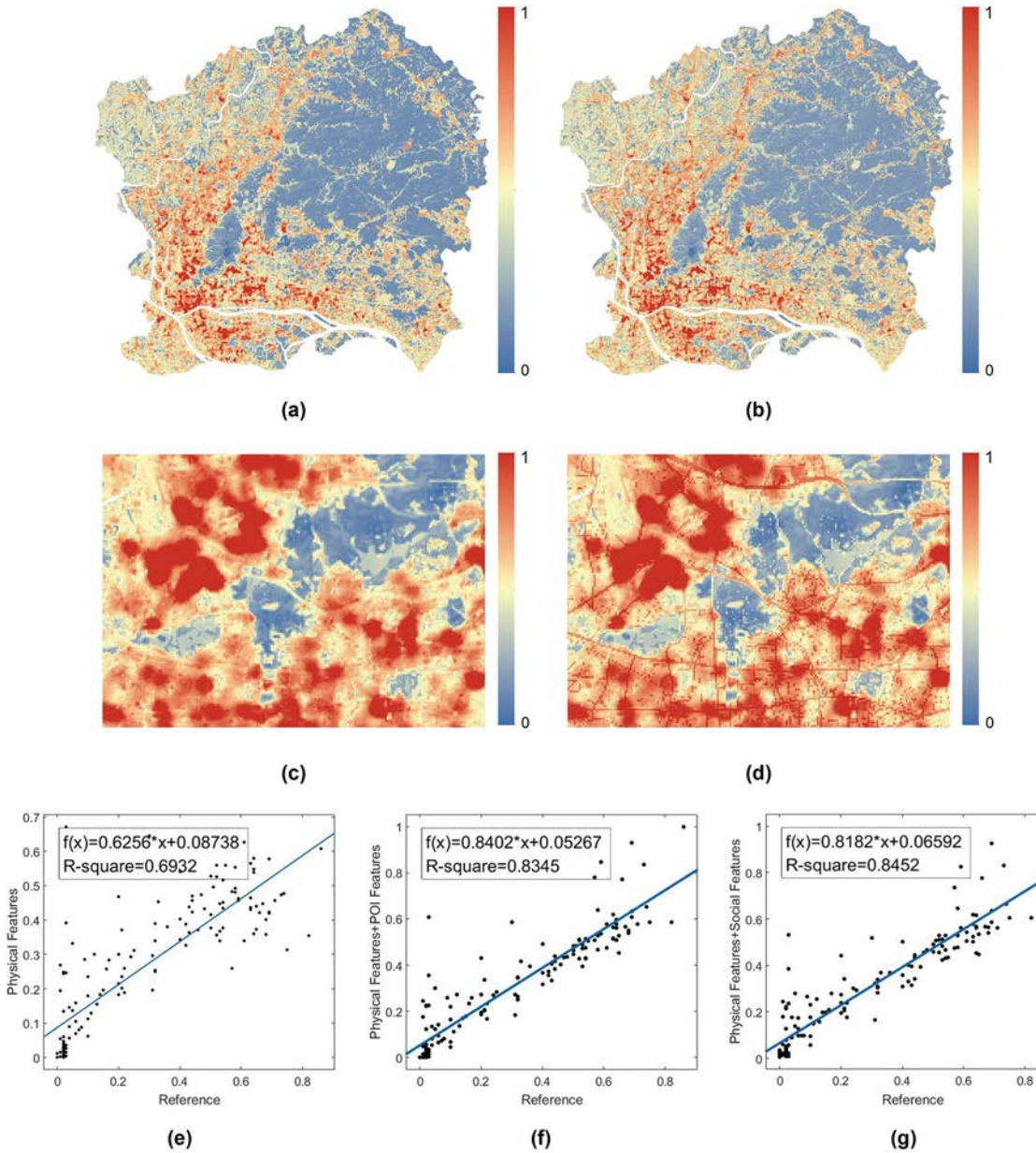

Figure 7. (a) impervious fractions estimated from physical features and POI features, and (b) estimated IS map integrating physical features, POI features and road distribution map; (c) and (d) are two zoomed-in view of (a) and (b), respectively. Fitting curves of (e) reference data versus physical features (R-square = 0.6932), (f) reference data versus IS result integrating physical and POI features (R-square = 0.8345), and (g) reference data versus impervious fractions integrating physical and all social features (R-square=0.8452), support the effectiveness of our method.

However, by taking advantage of social data, the impervious fractions can be well revised (see Figures 9c, and 9d).

We also calculated the histograms of bright imperviousness and dark imperviousness to explore whether our proposed method could well distinguish these two different land covers. 512 random samples of bright imperviousness (256 samples) and dark imperviousness (256 samples) are collected from *Gaode Map Online* manually. Figure 10 gives these histograms, in which the bright areas (blue line) and dark areas (read line) are well separated.

Several limitations still exist in our method. These are related with: (1) shadows, (2) the specific distribution of POIs, (3) the low density of pervious POIs, and (4) urban greening. These uncertainties are difficult to be fully avoided, especially with high spatial resolution imagery, which are exactly the aspects that we are planning to address in further studies.

Conclusions and Future Research

High spatial resolution and accurate estimation of impervious fractions are widely required in urban management. The accuracy of existing imagery-based IS estimation methods are usually hindered by the heterogeneity of remotely sensed imagery. To make progress in this direction, we exploited the unique advantages of social data to cover the shortages brought by traditional remote sensing imagery. A new approach which utilizes the combined strengths of remote sensing data and social data is proposed. Physical features of

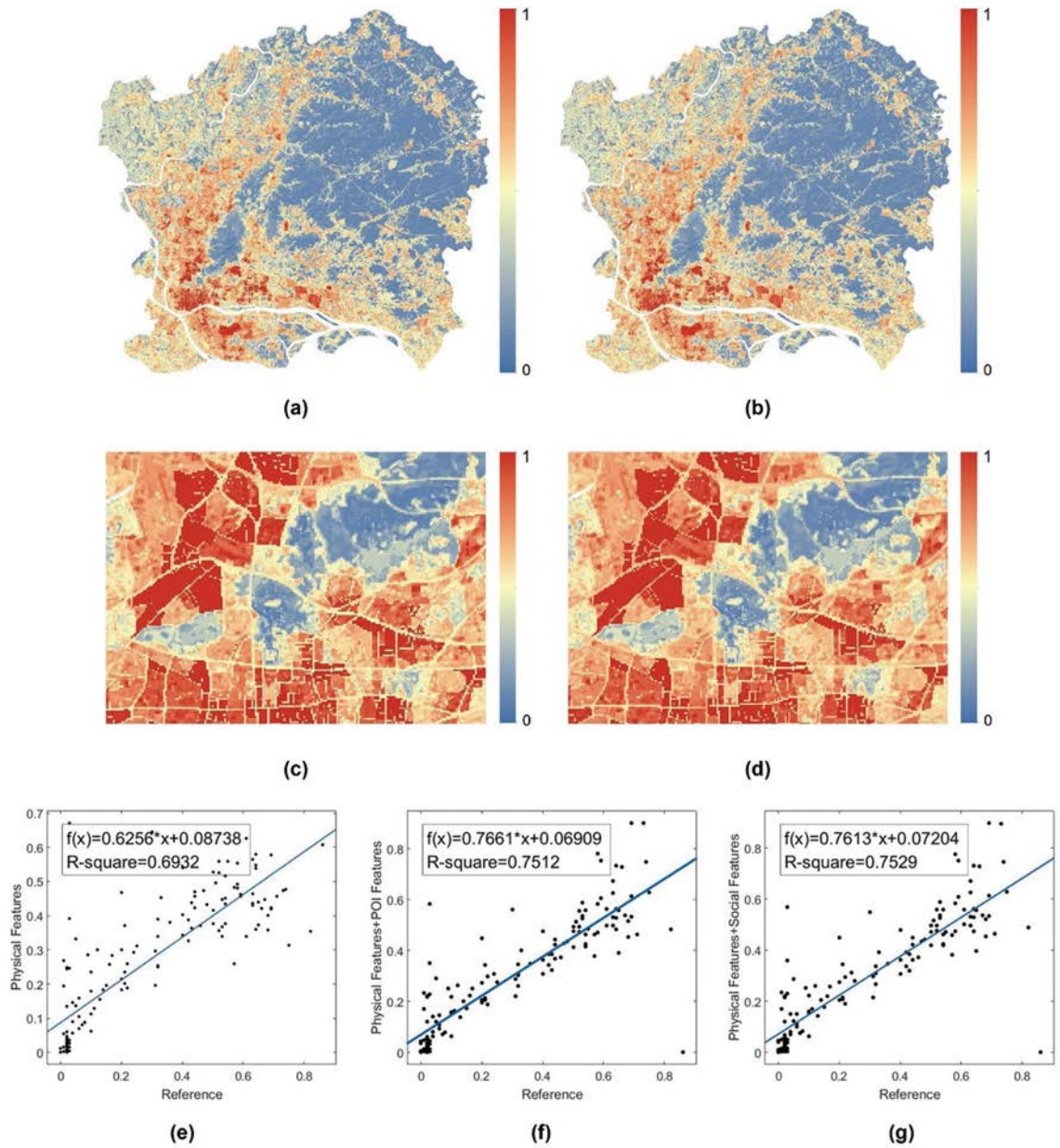

Figure 8. Parcel-based IS mapping result with (a) physical and POI features, and (b) physical and all social features; (c) and (d) are two zoomed-in views of two obtained maps, respectively, in which the high and low impervious fraction parcels are properly segmented; (e), (f) and (g) give the fitting curve of reference data versus impervious fractions, which are derived from physical features, physical and POI features, physical and all social features, respectively. The R-square of each figure is 0.6932, 0.7512, and 0.7529. Due to the low coverage rate of road network and the limited number of samples, the contributions made by road network are not easy to indicate by R-square.

IS derived from traditional remote sensing imagery contain physical characteristics of IS and basic map form, while social features generated from social data can provide abundant social information. Our protocol is shown to perform well in a case study focused on Guangzhou urban region in China, in which the overall RMSE reaches 10.98% and 10.90% for pixel level and parcel level, respectively. Though parcel-based IS map lost abundant details and has a relative lower accuracy comparing with pixel-based IS map, its social functions are well performed. Parcel-based IS map can be of great help to further investigation, such as detailed land use classification, built-up area extraction, and land use real-time monitoring. It is promising to apply this technique of both pixel-level and parcel-level into IS estimation in a relatively short time, especially in the suburban area and fast-growing countries.

There are several aspects in the proposed method that could be improved in future work. For instance, in this study, we used POI datasets collected from web maps, which are mostly located along the roads rather than uniformly distribute over the study area. This can lead to the inaccurate impervious fractions, as the fractions of pixels along the roads may be higher than the pixels inside, even if they belong to a same building. Volunteered POI/check-in data offered by social media platforms exhibit the potential to cover the shortage of POI data. Different from POI data, volunteered POI data are generated based on the location of users, but the social properties of these POIs are generally not defined. Additional efforts can be made by focusing on the identification and clustering of volunteered POI datasets to rationalize the impervious result. Another line of improvement is related to our utilization of a multivariable linear model for data fusion. Additional nonlinear models could be tested in future developments, like those based on neural networks, fuzzy set theories, Bayesian techniques, etc., (Zhang, 2010). These models exhibit potential to achieve even better performance in impervious surface mapping.

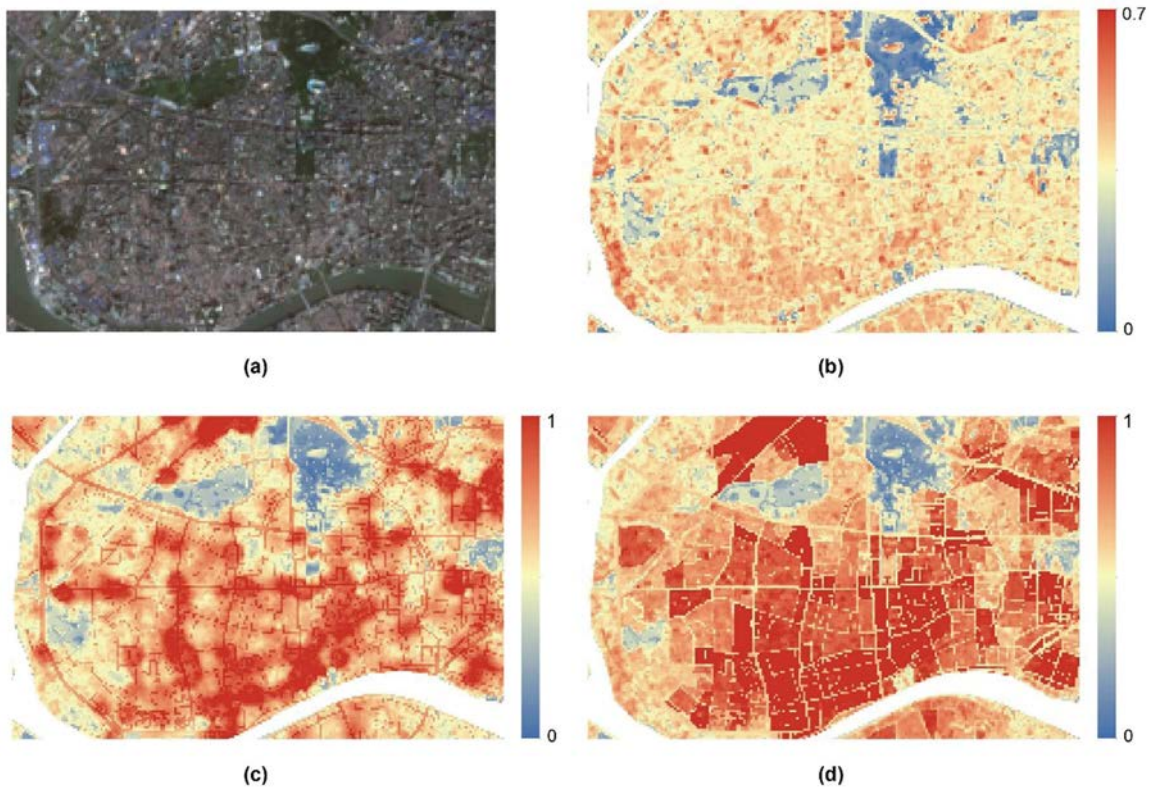

Figure 9. (a) Part of original imagery, (b) Physical features (initial impervious fractions derived by remote sensing imagery), (c) Pixel-based impervious surface estimation, (d) Parcel-based impervious surface estimation. The influences caused by urban greening are well avoided.

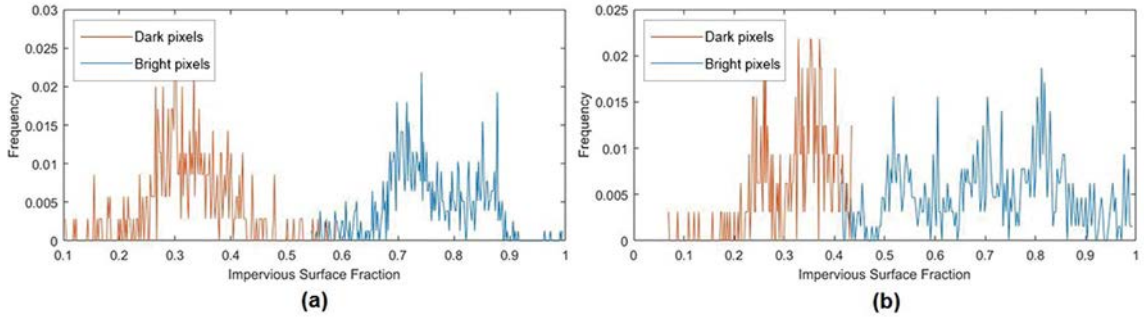

Figure 10. Histograms of bright imperviousness and dark imperviousness of (a) pixel-based result, and (b) parcel-based result.

Acknowledgments

This work was supported by the National Natural Science Foundation of China under Grant No.61771496; National Key Research and Development Program of China under Grant No.2017YFB0502900; Guangdong Provincial Natural Science Foundation under Grant No.2016A030313254.

References

Adams, J.B., M.O. Smith, and A.R. Gillespie, 1993. Imaging spectroscopy: Interpretation based on spectral mixture analysis, *Remote Geochemical Analysis: Elemental and Mineralogical Composition* (Carli M. Pieters, Peter A.J. Englert, editors), Cambridge University Press, Cambridge, UK, 7:145-166.

Arnold, Jr., C.L., and C.J. Gibbons, 1996. Impervious surface coverage: The emergence of a key environmental indicator, *Journal of the American Planning Association*, 62(2):243-258.

Arsanjani, J.J., M. Helbich, and M. Bakillah, 2013. Exploiting volunteered geographic information to ease land use mapping of an urban landscape, *Proceedings of the International Archives of the Photogrammetry, Remote Sensing and Spatial Information Sciences*, London, UK, pp. 29-31.

Bauer, M.E., N.J. Heinert, J.K. Doyle, and F. Yuan, 2004. Impervious surface mapping and change monitoring using Landsat remote sensing, *Proceedings of the ASPRS Annual Conference*, 18 - 23 May, Denver, Colorado (American Society for Photogrammetry and Remote Sensing, Bethesda, Maryland), 4:2334-2336.

Brabec, E., S. Schulte, and P.L. Richards, 2002. Impervious surfaces and water quality: A review of current literature and its implications for watershed planning, *CPL Bibliography*, 16(4):499-514.

Dalla Mura, M., J.A. Benediktsson, B. Waske, and L. Bruzzone, 2010. Morphological attribute profiles for the analysis of very high resolution images, *IEEE Transactions on Geoscience and Remote Sensing*, 48(10):3747-3762.

Deng, Y., F. Fan, and R. Chen, 2012. Extraction and analysis of impervious surfaces based on a spectral un-mixing method using Pearl River Delta of China Landsat TM/ETM+ imagery from 1998 to 2008, *Sensors*, 12(2):1846-1862.

Geiger, R., R.H. Aron, and P. Todhunter, 2009. *The Climate Near the Ground*, Rowman & Littlefield, Lanham, Maryland, 642 p.

Hasse, J.E. and R.G. Lathrop, 2003. Land resource impact indicators of urban sprawl, *Applied Geography*, 23(2):159-175.

Hu, T., J. Yang, X. Li, and P. Gong, 2016. Mapping urban land use by using Landsat images and open social data, *Remote Sensing*, 8(2):151.

Huang, X., D. Wen, J. Li, and R. Qin, 2017. Multi-level monitoring of subtle urban changes for the megacities of China using high-resolution multi-view satellite imagery, Remote Sensing of Environment, 196:56-75.

Jiang, S., A. Alves, F. Rodrigues, J. Ferreira, and F.C. Pereira, 2015. Mining point-of-interest data from social networks for urban land use classification and disaggregation, *Computers, Environment and Urban Systems*, 53:36-46.

Johnson, B.A., and K. Iizuka, 2016. Integrating OpenStreetMap crowdsourced data and Landsat time-series imagery for rapid land use/land cover (LULC) mapping: Case study of the Laguna de Bay area of the Philippines, *Applied Geography*, 67:140-149.

Li, P., J. Guo, B. Song, and X. Xiao, 2011. A multilevel hierarchical image segmentation method for urban impervious surface mapping using very high resolution imagery, l*EEE Journal of Selected Topics in Applied Earth Observations and Remote Sensing*, 4(1):103-116.

Liu, C., Z. Shao, M. Chen, and H. Luo, 2013. MNDISI: A multi-source composition index for impervious surface area estimation at the individual city scale, *Remote Sensing Letters*, 4(8):803-812.

Liu, Y., X. Liu, S. Gao, L. Gong, C. Kang, Y. Zhi, G. Chi, and L. Shi, 2015. Social sensing: A new approach to understanding our socioeconomic environments, *Annals of the Association of American Geographers*, 105(3):512-530.

Lu, D., and Q. Weng, 2006. Use of impervious surface in urban land-use classification, *Remote Sensing of Environment*, 102(1):146-160.

Lu, D., and Q. Weng, 2009. Extraction of urban impervious surfaces from an IKONOS image, *International Journal of Remote Sensing*, 30(5):1297-1311.

Lu, D., E. Moran, E., and S. Hetrick, 2011. Detection of impervious surface change with multitemporal Landsat images in an urban-rural frontier, *ISPRS Journal of Photogrammetry and Remote Sensing*, 66(3):298-306.

Lu, Y., and Y. Liu, 2012. Pervasive location acquisition technologies: Opportunities and challenges for geospatial studies, *Computers, Environment and Urban Systems*, 36(2):105-108.

Markham, B.L., and J.L. Barker, 1987. Thematic Mapper bandpass solar exoatmospheric irradiances, *International Journal of Remote Sensing*, 8(3):517-523.

Meng, Y., D. Hou, and H Xing, 2017. Rapid detection of land cover changes using crowdsourced geographic information: A case study of Beijing, China, *Sustainability*, 9(9): 1547.

Møller-Jensen, L., 1990. Knowledge-based classification of an urban area using texture and context information in Landsat-TM imagery, *Photogrammetric Engineering & Remote Sensing*, pp. 899-904.

Rodrigues, F., F.C. Pereira, A. Alves, S. Jiang, and J. Ferreira, 2012. Automatic classification of points-of-interest for land-use analysis, *Proceedings of Fourth International Conference on Advanced Geographic Information Systems, Applications, and Services*, 30 January-04 February, Valencia, Spain, pp. 41-49.

Sawaya, K.E., L.G. Olmanson, N.J. Heinert, P.L. Brezonik, and M.E. Bauer, M. E., 2003.

Extending satellite remote sensing to local scales: Land and water resource monitoring using high-resolution imagery, *Remote Sensing of Environment*, 88(1-2):144-156.

Schnebele, E., 2013. Improving remote sensing flood assessment using volunteered geographical data, *Natural Hazards and Earth System Sciences*, 13(3):669.

Schueler, T.R., 1994. The importance of imperviousness, *Watershed Protection Techniques*, 1(3):100-111.

Silverman, B.W., 1986. *Density Estimation for Statistics and Data Analysis*, 26, CRC Press, Boca Raton, Florida, 176 p.

Slonecker, E.T., D.B. Jennings, and D. Garofalo, 2001. Remote sensing of impervious surfaces: A review, *Remote Sensing Reviews*, 20(3):227-255.

Weng, Q., 2012. Remote sensing of impervious surfaces in the urban areas: Requirements, methods, and trends, *Remote Sensing of Environment*, 117:34-49.

Wu, C., and Murray, A. T., 2003. Estimating impervious surface distribution by spectral mixture analysis, Remote sensing of Environment, 84(4): 493-505.

Yang, L., C. Huang, C.G. Homer, B.K. Wylie, and M.J. Coan, 2003. An approach for mapping large-area impervious surfaces: Synergistic use of Landsat-7 ETM+ and high spatial resolution imagery, *Canadian Journal of Remote Sensing*, 29(2):230-240.

Yuan, F., and M.E. Bauer, 2007. Comparison of impervious surface area and normalized difference vegetation index as indicators of surface urban heat island effects in Landsat imagery, *Remote sensing of Environment*, 106(3):375-386.

Yuan, J., Y. Zheng, and X. Xie, 2012. Discovering regions of different functions in a city using human mobility and POIs, *ACM*, pp. 186-194.

Zhang, J., 2010. Multi-source remote sensing data fusion: Status and trends, *International Journal of Image and Data Fusion*, 1(1):5-24.

Zhang, T., and X. Huang, 2018. Monitoring of urban impervious surfaces using time series of high-resolution remote sensing images in rapidly urbanized areas: A case study of Shenzhen, *IEEE Journal of Selected Topics in Applied Earth Observations and Remote Sensing*, (99):1-17.

Zhu, C., J. Li, S. Zhang, C. Wu, B. Zhang, L. Gao, and A. Plaza, 2018. Impervious surface extraction from multispectral images via morphological attribute profiles based on spectral analysis, *IEEE Journal of Selected Topics in Applied Earth Observations and Remote Sensing*, Accepted, 2018.